Science
AAAS

Supplementary Materials for

Enterically derived high-density lipoprotein restrains liver injury via the portal vein

Yong-Hyun Han, Emily J. Onufer, Li-Hao Huang, Robert W. Sprung, W. Sean Davidson, Rafael S. Czepielewski, Mary Wohltmann, Mary G. Sorci-Thomas, Brad W. Warner, Gwendalyn J. Randolph

Correspondence to: gjrandolph@wustl.edu
yhhan1015@kangwon.ac.kr

This PDF file includes:

Supplementary Figures and Legends

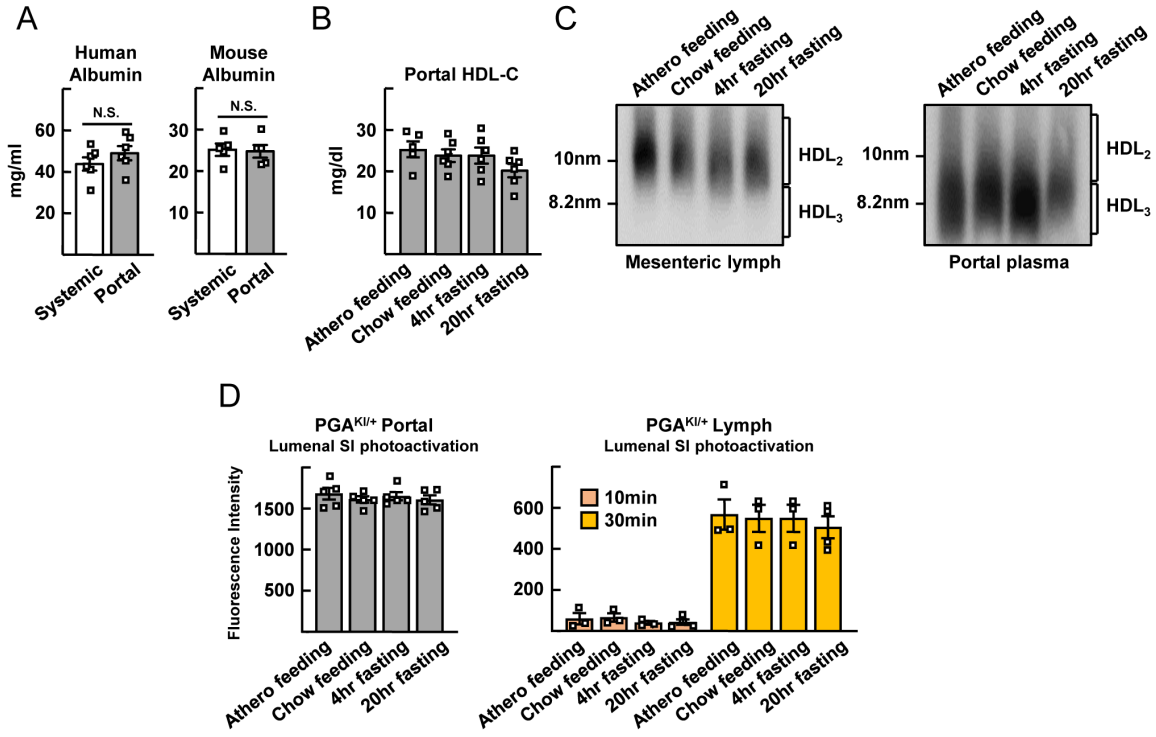

Figure S1. HDL status in relation to dietary feeding and fasting.
(**A**) Albumin levels of systemic and portal human or mouse plasma were measured. (**B-D**) Mice were fed with atherogenic (Athero) or standard chow diet, or fasted for 4 or 20 hours. **(B)** Portal HDL cholesterol levels. **(C)** Immunoblots for apoA1 run on a nondenaturing gel of mesenteric lymph and portal plasma samples from panel B. **(D)** The lumen of the small intestinal ileum (SI) of *Pga1*$^{KI/+}$ mice was photoactivated; portal plasma and mesenteric lymph fluorescence was assessed 5, 10, or 30 min later (portal blood, gray bars; lymph, yellow bars). All data are plotted as mean ± SEM analyzed by unpaired two-tailed Student's *t* test and include a mix of males and females, with each symbol on the bar graphs representing a single mouse or human.

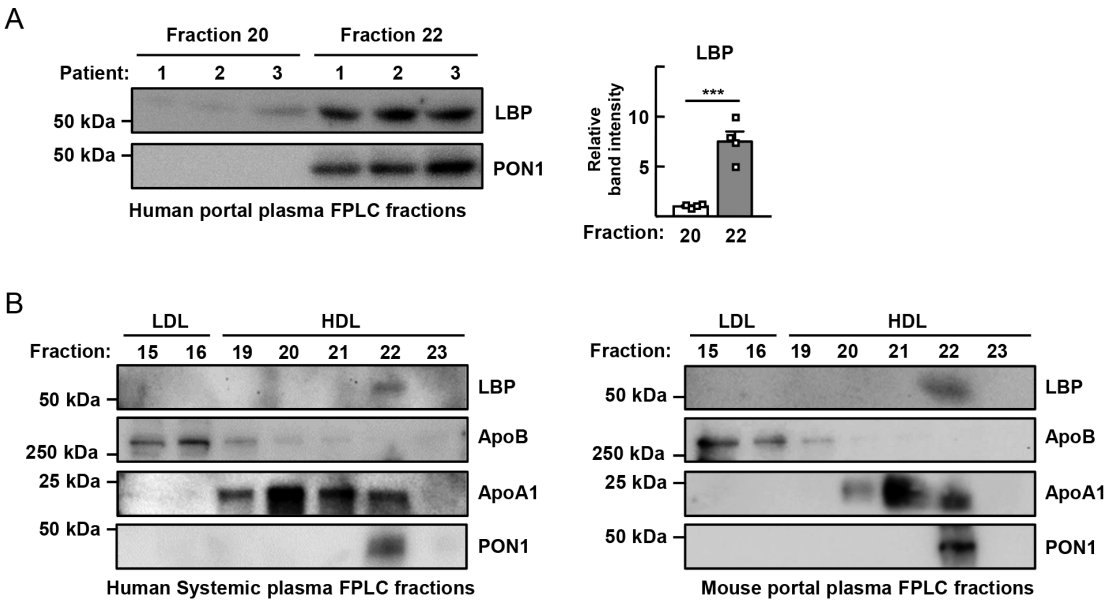

Figure S2. Plasma protein profiling in FPLC-separated fractions.

(A) Immunoblotting for LBP in three paired human samples after HDL was separated into fractions (fraction numbers shown) using size-exclusion chromatography. Fraction 20 contains the larger HDL_2, and fraction 22 the smaller HDL_3. Relative band intensity measured for four paired samples are graphically depicted on the right. **(B)** Human systemic and mouse portal plasma was separated by FPLC size-exclusion chromatography. LBP, apoB, apoA1, or PON1 in FPLC-separated fractions was analyzed by immunoblotting. Plots show mean ± SEM analyzed by paired two-tailed Student's *t* test. ***$P<0.001$

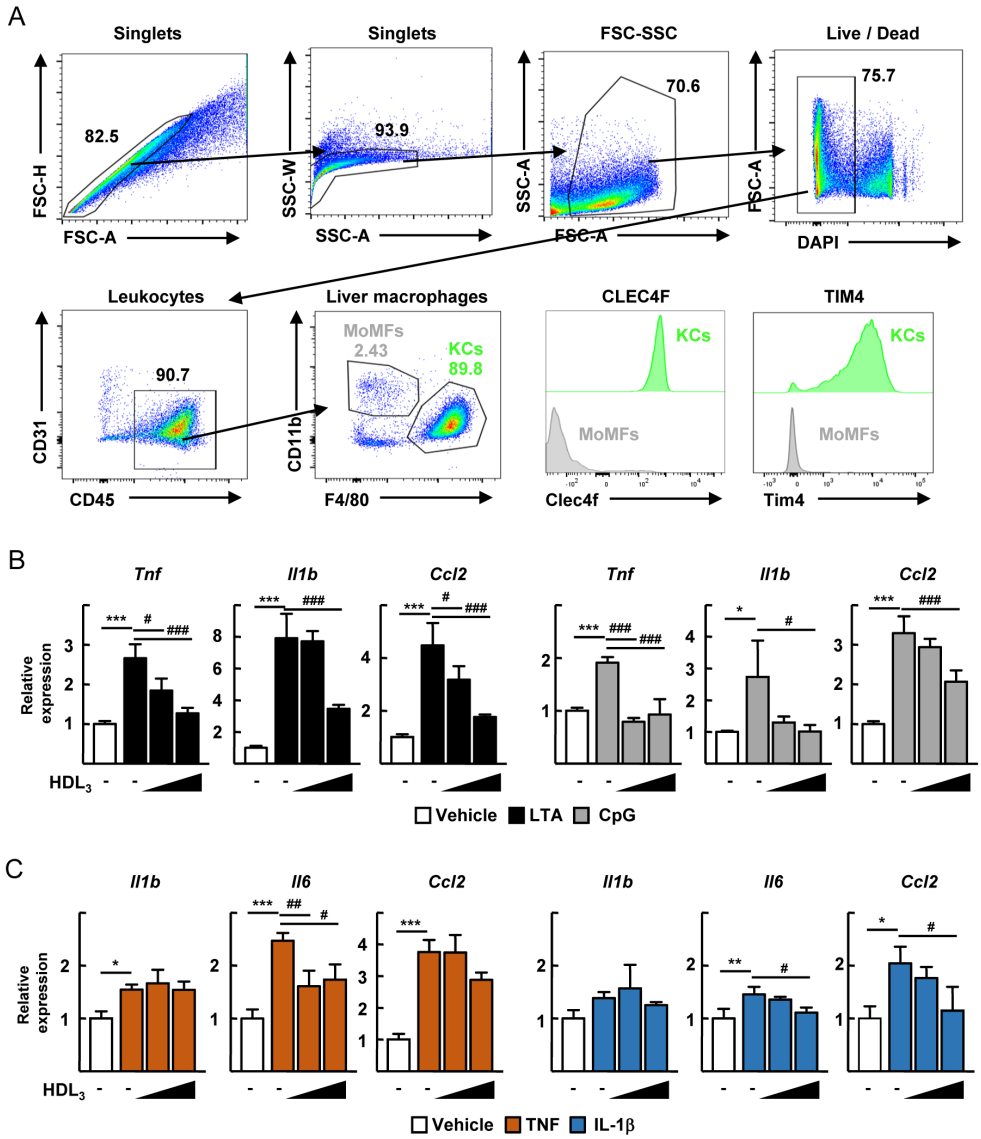

Figure S3. Gating strategy and inflammatory responses of liver Kupffer cells.
(**A**) Gating strategy and representative flow plots of liver macrophages, Kupffer cells (KCs), and monocyte-derived macrophages (MoMFs). Resident macrophage KCs accounted for approximately 80% of isolated cells. (**B**) 10 μg/ml of lipoteichoic acid (LTA) or CpG oligodeoxynucleotide-treated KCs was incubated in serum-free LBP-containing medium with or without HDL_3. (**C**) TNF- or IL-1β-treated KCs (each cytokine used at 100 ng/ml) was incubated in serum-free LBP-containing medium with or without HDL_3. The leftmost colored bar in each graph corresponds with data wherein HDL_3 was not included but the stimulus was (LTA, CpG, etc.); the second colored bar corresponds with addition of 20 μg/ml of HDL_3; the last colored bar with 100 μg/ml of HDL_3. Open bars show results with no inflammatory stimulus added to the KC cultures. mRNA transcripts of inflammatory genes measured by qRT-PCR. Plots show mean ± SEM analyzed by one-way ANOVA using a combination of male and female mice, with n=3-5 mice per time point, combined from at least two independent experiments. $^{*}P<0.05$; $^{**}P<0.01$; $^{***}P<0.001$; $^{\#}P<0.05$; $^{\#\#}P<0.01$; $^{\#\#\#}P<0.001$.

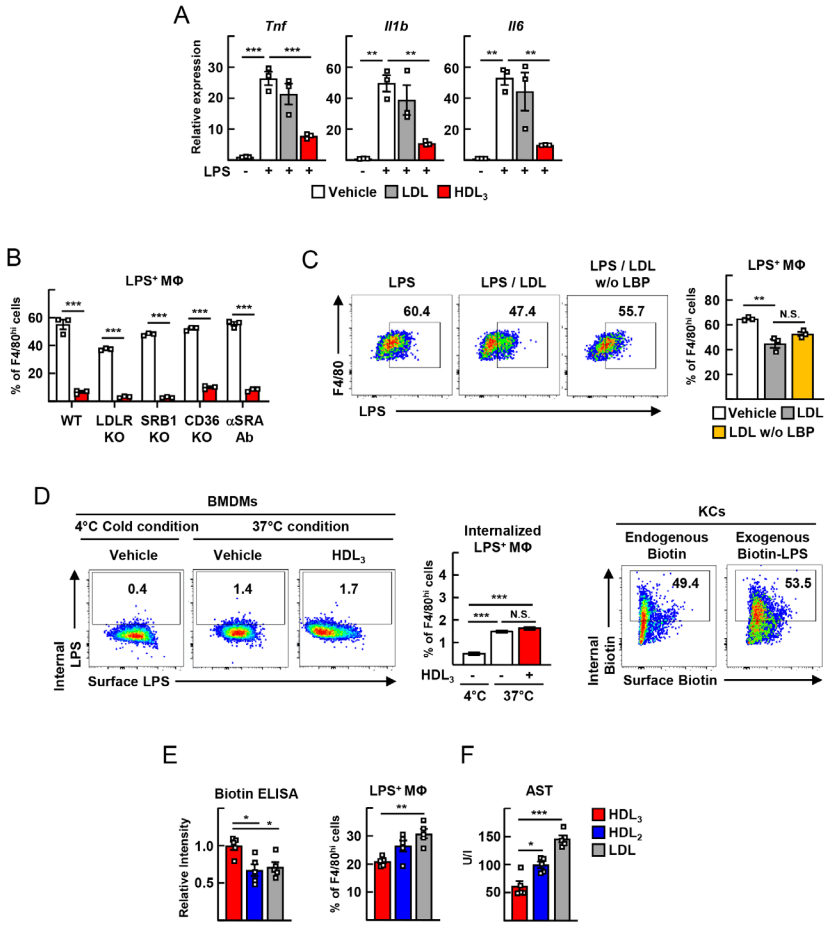

Figure S4. KC binding to LPS, effect of HDL or LDL on this binding, and inactivation of LPS carried by lipoproteins (**A**) KCs were incubated in serum-free LBP-containing medium with or without 20 ng/ml of LPS and 100 µg/ml of LDL or HDL_3 and mRNA transcripts of inflammatory genes were measured by qRT-PCR. (**B**) Bone marrow-derived macrophages (BMDMs) or KCs obtained from WT, LDLR, SRB1, or CD36 knockout mice were incubated with LBP and HDL_3 in the presence of biotin-LPS. SRA was neutralized using an antibody. (**C**) KCs were incubated with LDL with or without LBP in the presence of biotin-LPS and analyzed by flow cytometry. (**D**) BMDMs (left) were cultured and studied here rather than KCs (right), which had a very high endogenous biotin content (right panel). BMDMs supported surface binding of biotin-LPS and this was inhibited by HDL_3, as observed in KCs. Internalized biotin-LPS was detected in permeabilized cells and this was analyzed along with surface binding of biotin-LPS by flow cytometry. Less than 2% of BMDMs internalized LPS, even though surface binding at 37°C was evident by the right-shift on the x-axis of the flow plots when vehicle in the absence of HDL_3 was used. (**E** and **F**) HDL_3, HDL_2, or LDL complexed with equal amounts of biotin-LPS were injected to portal vein. Systemic plasma was harvested after 30 min. Biotin-LPS was measured by strepatavidin peroxidase ELISA (**E,** left). Cell surface binding of biotin-LPS in KCs was analyzed (**E,** right). Plasma AST levels were measured (**F**). Plots show mean ± SEM analyzed by unpaired two-tailed Student's *t* test [(B)] or one-way ANOVA [(A), (C), (D), (E) and (F)] using a combination of male and female mice, with n=3-5 mice per time point. Each symbol represents data obtained using a different mouse. **P*<0.05; ***P*<0.01; ****P*<0.001.

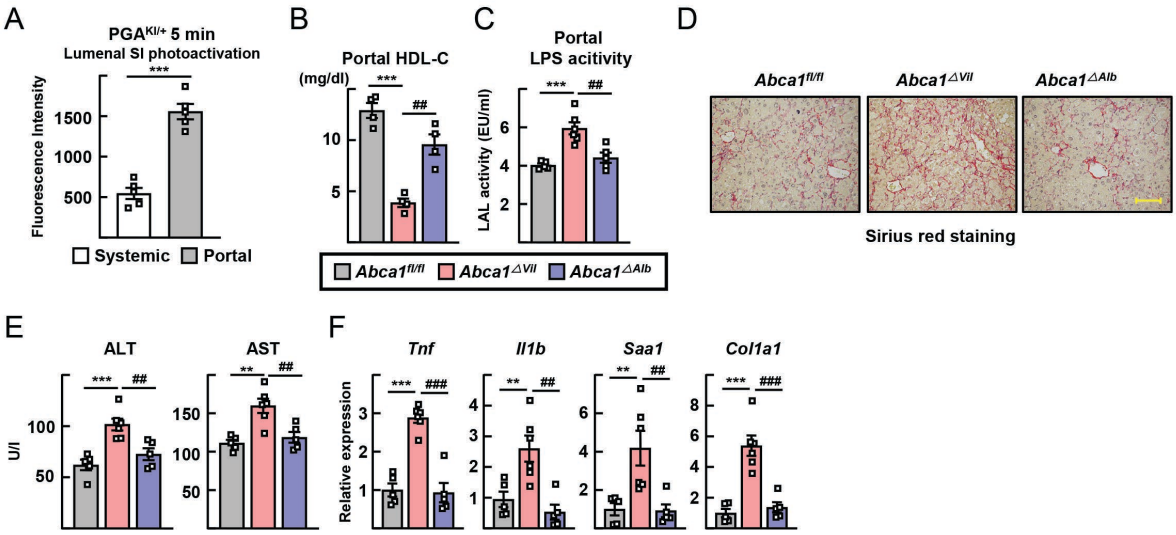

Figure S5. SBR-induced liver injuries in female mice with conditional deletion of Abca1. (**A**) The lumens of the small intestinal ileum (SI) of female *Pga1*$^{KI/+}$ mice were photoactivated; portal plasma was assessed 5 min later. (**B** to **F**) 75% short bowel resection (SBR) operations were performed on *Abca1*$^{fl/fl}$ (n=5), *Abca1*$^{\Delta Vil1}$ (n=6), and *Abca1*$^{\Delta Alb1}$ (n=5) mice and mice were euthanized 10 weeks later. (**B**) Portal HDL cholesterol levels. (**C**) Portal LPS activity assessed by LAL assay. (**D**) Representative images of Sirius red staining of liver sections. Scale bar: 100 μm. (**E**) Plasma ALT and AST levels. (**F**) Hepatic mRNA transcripts of inflammatory genes. Plots show mean ± SEM analyzed by unpaired two-tailed Student's *t* test [(A)] or one-way ANOVA [(B) to (F)] in female mice, with each symbol on the bar graphs representing a single mouse. $^{**}P<0.01$; $^{***}P<0.001$; $^{\#\#}P<0.01$; $^{\#\#\#}P<0.001$.

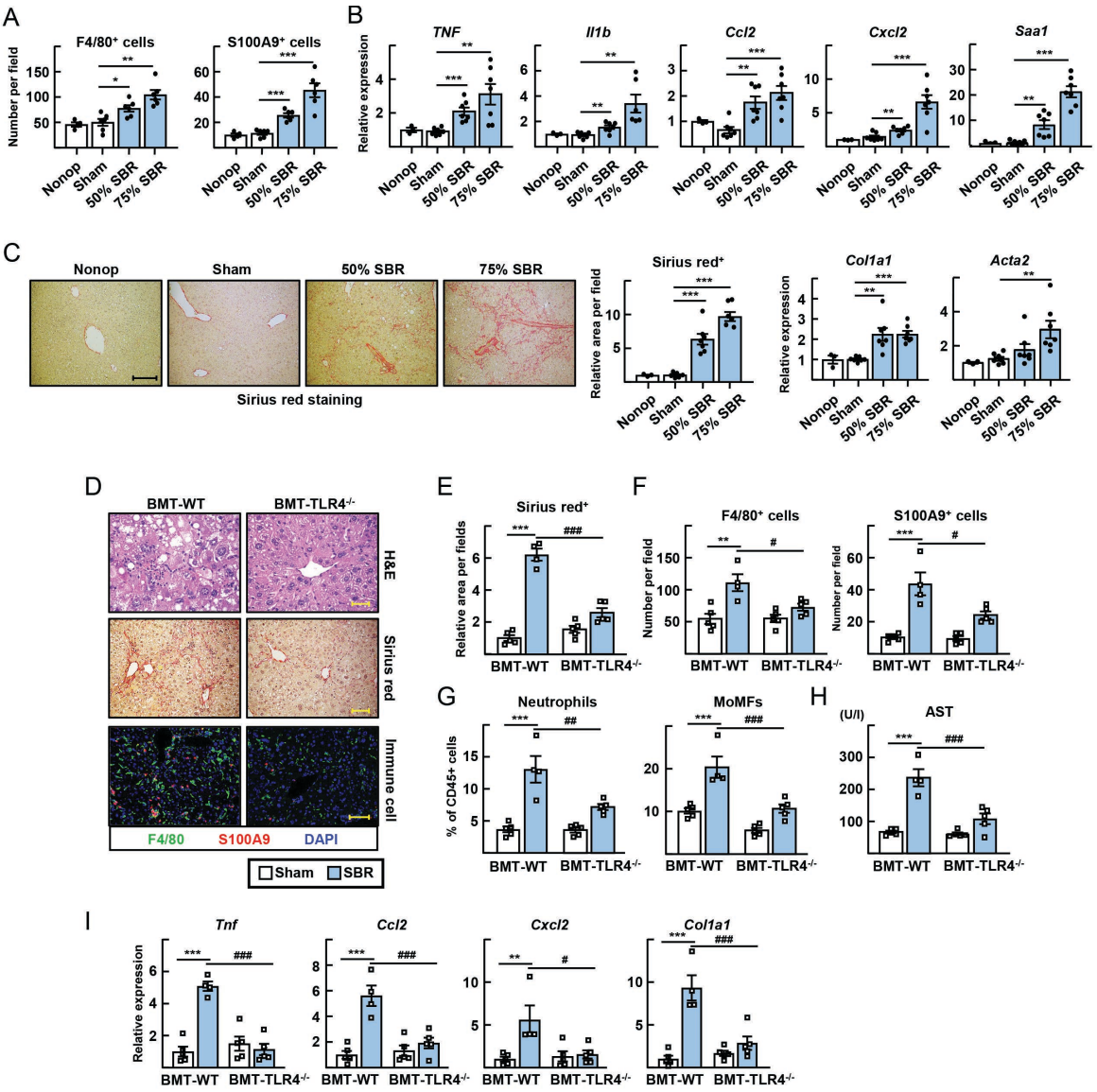

Figure S6. SBR-induced liver injury after bone marrow transplant of WT or *Tlr4*$^{-/-}$ hematopoietic cells into WT hosts. (**A** to **C**) Small bowel resection (SBR) operations were carried out on WT mice. Non-operated (Nonop) (n=4), sham (n=8), 50% SBR (n=8), or 75% SBR (n=8) mice were euthanized 12 weeks later. (**A**) Numbers of F4/80^{+} macrophages and S100A9^{+} neutrophils per high power field were counted. (**B**) Quantification of mRNA for inflammatory genes by qRT-PCR. (**C**) Representative images of Sirius red-stained liver sections (left). Scale bar: 200 μm. Quantification of mRNA for *Col1a1* and *Acta2* analyzed by qRT-PCR (right). (**D** to **I**) Mice receiving bone marrow transplants with WT or *Tlr4*$^{-/-}$ hematopoietic cells were later subjected to sham surgery or 75% short bowel resection and euthanized 10 weeks later. H&E, sirius red, and immunostaining of liver sections. Scale bar: 50 μm (top) or 100 μm (middle and bottom) (**D**). Relative sirius red positive area per field (**E**). Numbers of F4/80^{+} macrophages and S100A9^{+} neutrophils per field (**F**). The proportions of hepatic neutrophils and monocyte-derived macrophages (MoMFs) among CD45^{+} leukocytes (**G**). Plasma AST levels (**H**). Hepatic mRNA transcripts of inflammatory genes analyzed by qRT-PCR (**I**). Plots show mean ± SEM analyzed by one-way ANOVA in male mice, with each symbol on the bar graphs representing a single mouse. **P*<0.05; ***P*<0.01; ****P*<0.001; $^{\#}$*P*<0.05; $^{\#\#}$*P*<0.01; $^{\#\#\#}$*P*<0.001.

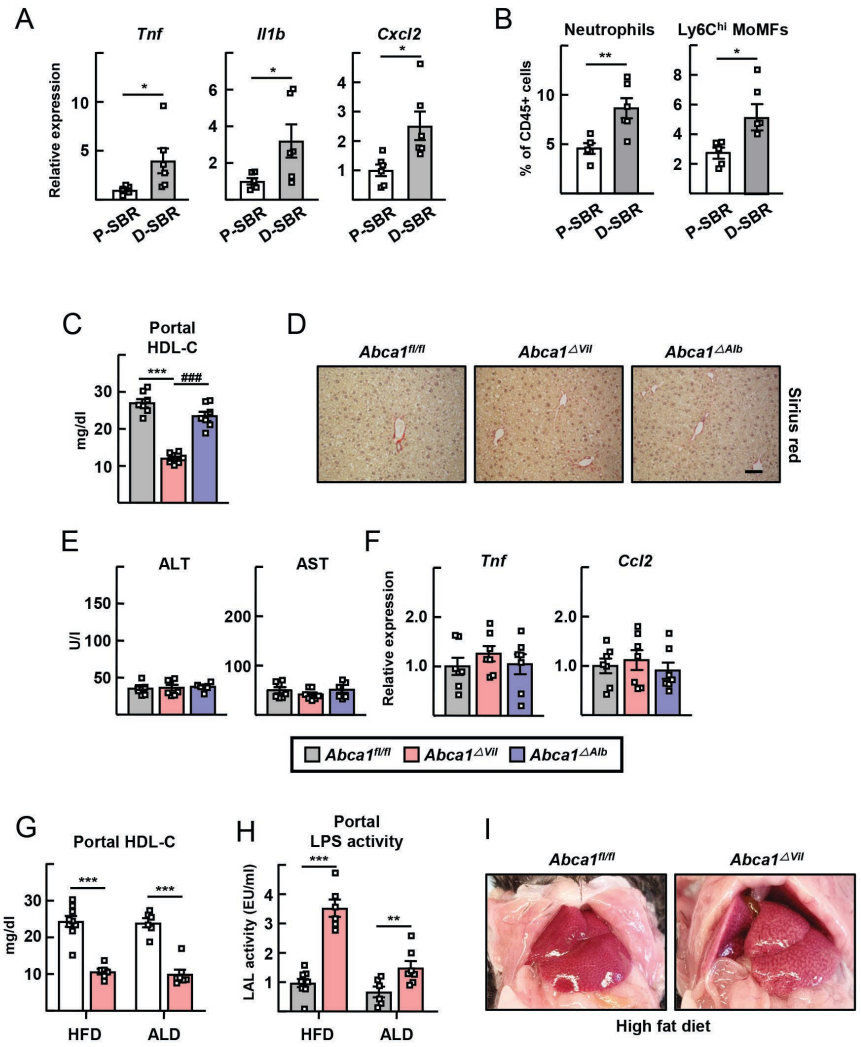

Figure S7. Evaluation of liver injury in response to distal bowel resection, sham operation, high fat diet or alcoholic Lieber-DeCarli diets. (**A and B**) SBR operations were conducted on WT mice. Mice receiving proximal 50% SBR (P-SBR) (n=6), or distal 50% SBR (D-SBR) (n=6) operations were euthanized 10 weeks later. (**A**) Hepatic mRNA transcripts of inflammatory genes. (**B**) The proportions of hepatic neutrophils and Ly6C^{hi} monocyte-derived macrophages (MoMFs) among CD45^{+} leukocytes. (**C** to **F**) Sham operations were carried out on *Abca1*$^{fl/fl}$ (n=7), *Abca1*$^{\Delta Vil1}$ (n=7), and *Abca1*$^{\Delta Alb1}$ (n=7) mice, which were euthanized 8 weeks later. (**C**) Portal HDL cholesterol levels. (**D**) Representative images of sirius red staining of liver sections. Scale bar: 100 µm. (**E**) Plasma ALT and AST levels. (**F**) Hepatic mRNA transcripts of inflammatory genes. (**G** to **I**) *Abca1*$^{fl/fl}$ and *Abca1*$^{\Delta Vil1}$ mice were fed a high-fat diet (HFD) (n=9 *Abca1*$^{fl/fl}$; n=6 *Abca1*$^{\Delta Vil1}$) or alcohol-containing diet (ALD) (n=6 *Abca1*$^{fl/fl}$; n=7 *Abca1*$^{\Delta Vil1}$). (**G**) Portal HDL cholesterol levels. (**H**) Portal LPS activity assessed by LAL assay. (**I**) Representative pictures of intact livers after HFD. Plots show mean ± SEM analyzed by unpaired two-tailed Student's *t* test [(A), (B), (G) and (H)] or one-way ANOVA [(C)] in male mice, with each symbol on the bar graphs representing a single mouse. *P<0.05; **P<0.01; ***P<0.001; $^{\#\#\#}$P<0.001.

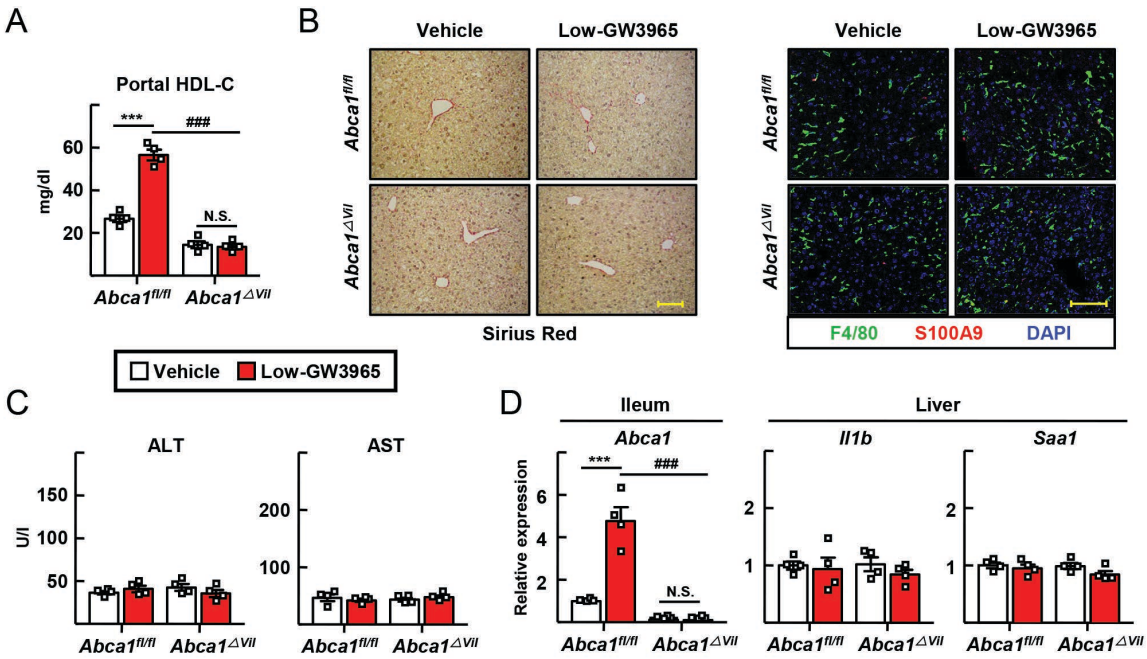

Figure S8. Effect of low-dose GW3965 on the liver response. (**A**) *Abca1*$^{fl/fl}$ and *Abca1*$^{\Delta Vil1}$ mice received vehicle (n=10 *Abca1*$^{fl/fl}$; n=8 *Abca1*$^{\Delta Vil1}$) or 1 mg/kg/day GW3965 (n=10 *Abca1*$^{fl/fl}$; n=8 *Abca1*$^{\Delta Vil1}$) by gavage twice weekly in the last 5 weeks of a 10-week feeding following SBR (Low-GW3965). mRNA transcripts of LXR target genes in ileum, liver, and peritoneal cells were measured by qRT-PCR. (**B**) Representative image of ABCA1 (green) and F4/80 (red) immunostaining of ileum sections. Scale bar: 50 µm. (**C**) *Abca1/g1*$^{fl/fl}$ and *Abca1/g1*$^{\Delta Lyz2}$ mice received vehicle (n=5 mice per genotype) or 1 mg/kg/day GW3965 (n=5 mice per genotype) by gavage twice weekly for 5 weeks. Portal HDL cholesterol levels are shown on the left, and mRNA transcripts of *Abca1* in ileum tissues analyzed by qRT-PCR on the right. All data are plotted as mean ± SEM analyzed by one-way ANOVA in male mice, with each symbol on the bar graphs representing a single mouse. **P*<0.05; ***P*<0.01; ****P*<0.001.

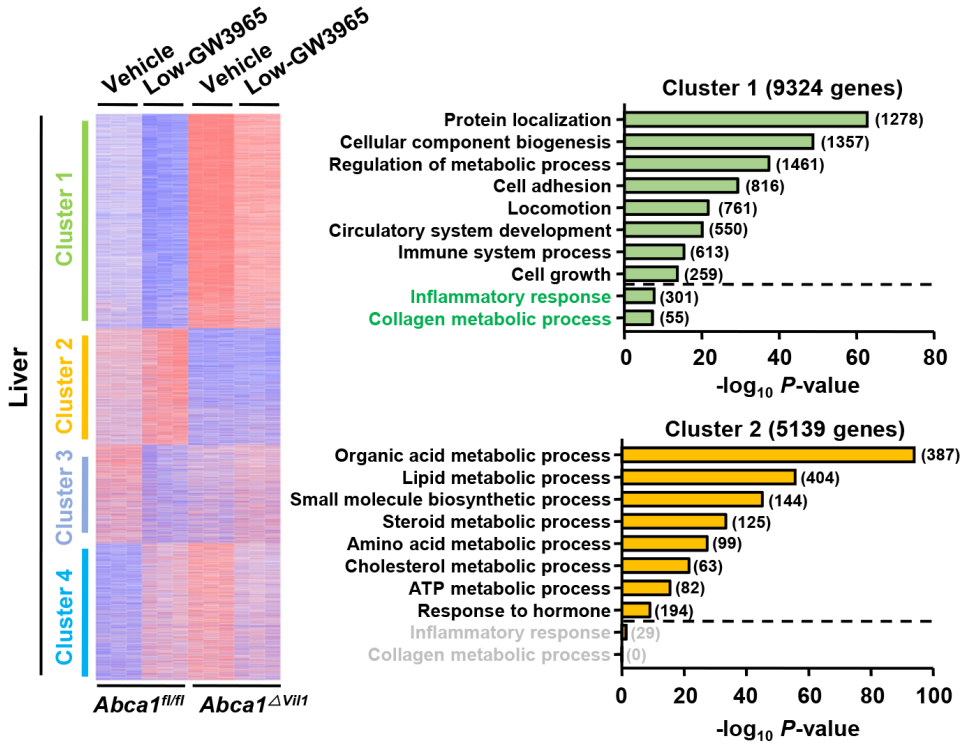

Figure S9. Gene ontology pathways identified in the liver after oral, low-dose GW3965 treatment

Global heat map of mRNA transcripts differentially expressed in liver tissue (left). Gene ontology pathways associated with cluster 1 and 2 genes are detailed on the right. Log_{10} adjusted *P*-value is shown on the *x*-axis and the number of genes associated with the pathway is given in parentheses next to the bar corresponding to a particular pathway.

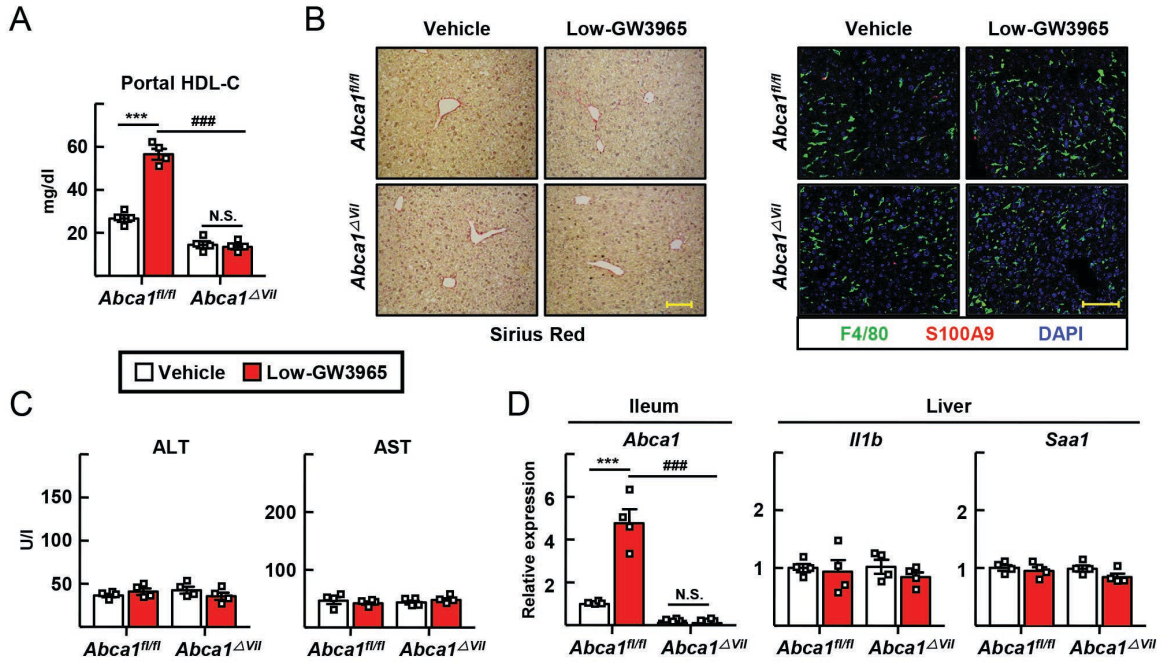

Figure S10. Evaluation of liver injury in sham-operated control mice with or with GW3965 treatment.

Abca1$^{fl/fl}$ and *Abca1*$^{\Delta Vil1}$ mice received vehicle (n=4 mice per genotype) or 1 mg/kg/day GW3965 (n=4 mice per genotype) by gavage twice weekly in the last 5 weeks of a 10-week feeding following sham operation (Low-GW3965). (**A**) Portal HDL cholesterol levels are shown. (**B**) Representative images of Sirius red staining of liver sections are shown on the left, and representative images of F4/80^{+} macrophages and S100A9^{+} neutrophils visualized by immunofluorescence staining on the right. Scale bars: 100 μm. (**C**) Plasma ALT and AST levels. (**D**) Ileum and liver mRNA transcripts were analyzed. Plots show mean ± SEM analyzed by one-way ANOVA in male mice, with each symbol on the bar graphs representing a single mouse. ***P<0.001; $^{###}P$<0.001.

Caption to Table S1.

A list of proteins associated with HDL_2 or HDL_3 derived from different venous locations and their quantitative values identified using proteomics.

Table S2. Antibodies used, their source, and dilutions

Use	Targets	Vendors	Catalog numbers	Conjugates	Dilution	Species
Immuno-staining	F4/80	Abcam	ab6640	None	1:100	Mouse
	S100A9	R&D systems	AF2065	None	1:10000	Mouse
	vWF	DAKO	a0082	None	1:200	Mouse
	PV1	BD Pharmingen	550563	None	1:200	Mouse
	ABCA1	Novus Biologicals	NB400-105	None	1:100	Mouse
Immuno-blots	apoA1	Meridian Life Sciences	K23001R	None	1:5000	Mouse
	apoA1	Millipore	MAB011	None	1:5000	Human
	ABCA1	Novus Biologicals	NB400-105	None	1:2000	Human
	PON1	Abcam	ab24261	None	1:2000	Mouse, Human
	apoB	Proteintech	20578-1	None	1:4000	Mouse, Human
	LBP	Abcam	ab2333524	None	1:3000	Mouse, Human
	AOAH	Proteintech	12911-1	None	1:3000	Mouse, Human
	SERPIN A1	Thermo Fisher	PA5-16661	None	1:5000	Mouse, Human
	ApoE	D.M. Holztmann (Washington University)		None	1:5000	Mouse, Human
	Albumin	Proteintech	16475-1	None	1:2000	Mouse, Human
Flow	CD45	BD biosciences	563791	BUV396	1:500	Mouse

cytometry	Ly6G	Biolegend	127605	FITC	1:300	Mouse
	F4/80	Biolegend	123117	APC/Cy7	1:300	Mouse
	Ly6C	Biolegend	128011	PerCP/Cy5.5	1:200	Mouse
	CD31	Biolegend	102417	PE/Cy7	1:300	Mouse
	iNOS	Thermo Fisher	53-5920-82	Alexa 488	1:200	Mouse
	CD11b	Thermo Fisher	17-0112-81	APC	1:300	Mouse
	Tim4	Thermo Fisher	12-5866-82	PE	1:300	Mouse
	Clec4f	R&D systems	AF2784	None	1:100	Mouse
	Strept-avidin	Biolegend	405206	PE/Cy7	1:200	
	Strept-avidin	Biolegend	405229	BV605	1:200	